coatings

MDPI

Article

Design of Benzoxazine Coatings to Further Advance Acid Resistance of Aluminium Substrates

Louis Van Renterghem [1], Roya Malekkhouyan [2], Leila Bonnaud [1,*], Marie-Georges Olivier [2] and Jean-Marie Raquez [1,*]

[1] Laboratory of Polymeric and Composite Materials (LPCM), Center of Innovation and Research in Materials, Materia Nova Research Center, University of Mons (UMONS), Place du Parc 20, 7000 Mons, Belgium; louis.vanrenterghem@umons.ac.be

[2] Materials Science Department, Materials Institute, University of Mons, Place du Parc 20, 7000 Mons, Belgium; roya.malekkhouyan@umons.ac.be (R.M.); marjorie.olivier@umons.ac.be (M.-G.O.)

* Correspondence: leila.bonnaud@materianova.be (L.B.); jean-marie.raquez@umons.ac.be (J.-M.R.); Tel.: +32-(0)65-55-49-75 (L.B.)

Abstract: Polybenzoxazine (PBz) resins exhibit excellent mechanical, thermal, and adhesive properties, making them interesting candidates for coating applications. Moreover, thanks to the incorporation of exchangeable ester bonds within the PBz network, the coating presents healable properties that are catalyzed by the intrinsic presence of tertiary amine within the PBz backbone. Unfortunately, these tertiary amine functions are also responsible for the limited resistance of such systems to acid environments by protonation. To address this limitation, the protection of tertiary amines inherent to the PBz network was investigated in this study by incorporating an aromatic group close to the amine function to minimize its protonation via hindrance/mesomeric effects. More precisely, benzoxazine precursors based on monoethanolamine (mea) and aminophenylethyl alcohol (Apa) were synthesized and tested as protective coatings of aluminium alloy substrates (AA1050). The resins were characterized by NMR, FTIR, rheology, TGA, DSC, and DMA. PBz synthesized from Apa exhibits enhanced thermal stability, reduced swelling rates in both water and acid, and shortened relaxation times. After application via solvent casting on AA1050 substrates, the acid resistance of the coatings was evaluated. Electrochemical impedance spectroscopy results demonstrated better resistance of the Apa-based resins in 0.1 M sulfuric acid after one month of immersion.

Keywords: benzoxazine; aluminium alloy; polymer coatings; acid resistance

Academic Editor: Frederic Sanchette

Received: 12 December 2024
Revised: 21 December 2024
Accepted: 24 December 2024
Published: 9 January 2025

Citation: Van Renterghem, L.; Malekkhouyan, R.; Bonnaud, L.; Olivier, M.-G.; Raquez, J.-M. Design of Benzoxazine Coatings to Further Advance Acid Resistance of Aluminium Substrates. *Coatings* **2025**, *15*, 67. https://doi.org/10.3390/coatings15010067

1. Introduction

In recent years, aluminium (Al) alloys have been used in widespread applications like aircraft or automobiles [1,2]. Al alloys have a low density, which can reduce the overall weight of the equipment and consequently the fuel consumption [2]. Moreover, Al alloys can be used in applications that require high strength and hardness. Aside from these properties, Al alloys have proper workability, castability, machinability, and recyclability, as well as fatigue and corrosion resistance [3,4]. In atmospheric conditions, an oxide layer (Al_2O_3) can be formed on the surface of Al alloy and decrease the corrosion rate [5]. However, in the presence of saline, alkaline, or acidic solutions, corrosion can be considerably increased [6].

The main strategy to limit Al alloy corrosion consists of isolating the metal from corrosive media. When the use of inorganic corrosion inhibitors such as phosphates,

chromates, and arsenates is severely limited due to their toxicity [7–9], the application of a protective organic coating appears to be the best alternative. Such coatings act as a barrier against aggressive species and reduce environmental damage to the substrate [10]. Although there is extensive literature on improving the corrosion resistance of aluminium alloys with polybenzoxazine coatings in saline solutions [11,12], there are only a limited number of studies that have examined the chemical resistance of these coatings to the aluminium substrate, particularly in the case of acid attacks [13,14].

Acid-resistant coatings are of great interest, as they can be used to protect ceramic and metallic substrates in industries that produce and consume acids. However, the use of acid-resistant organic coatings is often limited by industrial process variables such as temperature, pH, type, and concentration of acid. Thermoset coatings can protect substrates by forming a 3D network when cured and cross-linked. Therefore, the acid resistance of thermoset organic coatings depends on the network structure. Although several organic resins such as polyurethane [15], epoxy [16], polyaniline [17], and polypyrrole [18] have been used to protect aluminium alloys from salt media, the effect of acids within this network was poorly explored in the literature to the best of our knowledge. However, chemical and physical degradation of organic coatings in an acidic environment is known to occur. In the case of physical degradation, chemicals diffuse through the coating, while in the case of chemical degradation, chemicals react with the coating. The poor corrosion resistance of organic coatings is usually due to the diffusion of chemicals (physical degradation) and the attack of the H^+ proton on the alkaline moieties, such as amine, carried by the macromolecule (chemical degradation). Lim et al. [19] showed the acid degradation mechanism for an epoxy system. This aggression comes from the plasticization of the system due to the protonation of tertiary amine present in the macromolecules [19]. Due to protonation, swelling occurs, leading to physical erosion and structure degradation.

Following this concept, one approach to consider would be the protection against acid-sensitive groups. Interestingly, benzoxazine (BZX) resins allow for the design of a wide variety of network structures, making them the best candidates for the development of acid-resistant organic systems [20]. In addition, BZX is suitable for protecting metallic substrates because it interacts well with metal and OH phenols [3,11,12,21]. Moreover, the possibility to tune the flexibility of the benzoxazine backbone serves to enhance its capacity to adhere to metallic substrates [22]. Their low dielectric constant, thermal stability, alkaline resistance, hydrophobic behavior, and the ease of introducing self-healing and re-processability features by incorporating dynamic bonding into the network [23,24] have recently attracted lot of attention for coating applications [25]. Benzoxazine precursors are typically produced through a simple reaction involving three reagents: a phenol, an amine, and formaldehyde. This reaction yields high amounts and is known for imparting exceptional properties to the resulting compounds [26]. Several biobased phenols have already been employed in the synthesis of benzoxazine precursors for coatings. For example, thymol [27], curcumin [28], cardanol [29], trihydroxystilbene [30], and lignin-based compounds [31] have been shown to possess effective anti-corrosive properties and good hydrophobicity. The thermosetting nature of polybenzoxazine resins has made them difficult to be recycled and repaired, even though these phenols are bio-based. Interestingly, by incorporating exchangeable bonds to transform the polybenzoxazine's three-dimensional structure into a dynamic covalent network, their durability can be improved. Many dynamic networks have been the subject of studies about polybenzoxazine resins [24,32–35]. Nevertheless, the transesterification via the exchange of ester and alcohol functions remains the most extensively researched and documented approach [24,36,37] due to the intrinsic presence of a tertiary amine in the network after polymerization, which acts as an internal catalyst [38]. To incorporate ester functions into the BZX network, it is possible to use phenols that have additional chemi-

cal functions such as an acid or an alcohol. Recently, our research group has developed phloretic acid (PA)-based polybenzoxazine networks for the protection of metal substrates, including aluminium (Al) and magnesium (Mg) alloys [24,37].

Phloretic acid is a naturally occurring phenolic compound that can be produced by hydrogenation of p-coumaric acid or derived from a by-product of apple tree leaves. It is a phenol bearing a carboxylic acid function in the para-position. Furthermore, this phenol is not substituted in the ortho-position, thus favoring the ring-opening polymerization of the resulting BZX precursors [39]. The ester functions were introduced through a reaction between the phenolic compound bearing an acid function (i.e., phloretic acid) and diols of varying molecular weights, specifically ethylene glycol and decandiol. To achieve transesterification and simultaneously reduce the crosslinking temperature of the precursors, an excess of hydroxyl functions was also incorporated into the polymer backbone by the use of monoethanolamine. Indeed, it is well known that hydroxyl functions accelerate the polymerization of benzoxazine systems [40]. Unfortunately, these resins are weak in acidic environments despite their good performance such as rapid relaxation and good corrosion resistance in neutral sodium chloride solution.

This research aims to develop benzoxazine precursors with excellent acid resistance and fast relaxation features. Inspired by the study by Kim [41], the protection of the tertiary amine inherent to the polybenzoxazine network was investigated through the mechanisms of mesomeric effect and steric hindrance. In this regard, two amines were selected for the synthesis of the aforementioned BZX resins. Initially, monoethanolamine (mea) was employed as a reference. The second amine, aminophenylethyl alcohol (Apa), was selected to enhance protection against acidic media. This primary amine contains an aromatic ring directly attached to the amine, which can protect against acid degradation by mesomeric effect and/or steric hindrance. In addition to durability enhancement, it is worth noting that they are also partially biobased, contributing to improved environmental impact.

2. Materials and Methods

2.1. Sample Preparation

2.1.1. Materials

Phloretic acid (>98%) was purchased from TCI. Ethylene glycol (99.8%), para-toluenesulfonic acid (98.5%), methyl ethyl ketone, paraformaldehyde, and 1.10 decandiol (98%) were obtained from VWR. Ethanolamine was acquired from Merck. Aminophenylethyl alcohol was purchased from Apollo Scientific. All chemicals were used without further purification.

2.1.2. Synthesis of Phloretic Ester

The synthesis of PA-decandiol (PA-DD) and PA-ethylene glycol (PA-EG) was performed according to Figure 1. The operating conditions were the same for all the samples, according to the procedures described in an earlier report [38]. The synthesis protocol for the PA-DD is explained as an example. Phloretic acid (120 mmol), an excess of 1,10-decandiol (72 mmol), and paratoluenesulfonic acid (1 mmol) were placed into a 250 mL beaker equipped with a stirring bar. The mixture was stirred at 130 °C for 24 h at 150 rpm. After cooling to room temperature, the crude product was solubilized in 200 mL of methyl ethyl ketone. Then, the solution was washed with deionized water three times to remove the catalyst and the excess of diols. The organic solvent was dried under vacuum overnight to obtain a dark red viscous liquid yield of 95%; 1H-NMR (DMSO-d6, ppm): PA-dd: 9.14 (Ar–OH*), 7.00 (Ar*–OH), 6.65 (Ar*–OH), 3.97 (O=C–O–CH2*), 2.74 (HO–AR–CH2*), 2.53 (HO–AR–CH2–CH2*), 1.50 (O=C–O–CH2–CH2*), 1.25 (DD–CH2*–CH2*–). PA-EG: 9.17

(Ar–OH*), 7.02 (Ar*–OH), 6.67 (Ar*–OH), 4.19 (O=C–O–CH2*), 2.74 (HO–AR–CH2*), and 2.56 (HO–AR–CH2–CH2*).

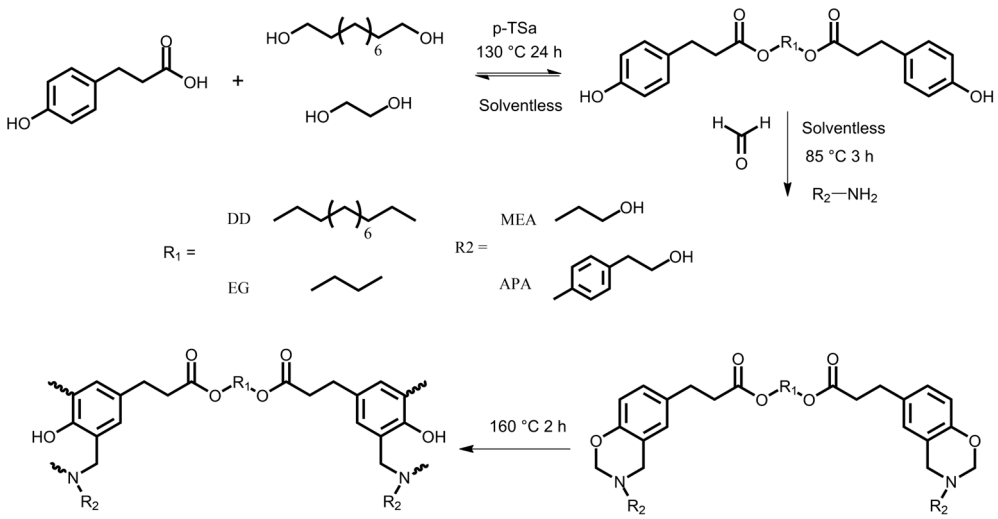

Figure 1. Synthesis of pPA-DD-mea, pPA-DD-Apa, pPA-EG-mea, and pPA-EG-Apa.

2.1.3. Synthesis of Phloretic Benzoxazine

The syntheses of PA-DD-mea, PA-DD-Apa, PA-EG-mea, and PA-EG-Apa were performed according to Figure 1. The operating conditions were the same for all samples. The synthesis protocol for the PA-DD-mea is detailed as an example. Phloretic ester (58.5 mmol), primary amine (117 mmol), and paraformaldehyde (234 mmol) were placed into a 250 mL beaker equipped with a stirring bar. The mixture was stirred at 85 °C for 150 min and 30 min at 90 °C at 150 rpm. The resulting product was a dark red viscous liquid. The assignment of each nuclear magnetic resonance peak and the integral values can be found in the supplementary information. FTIR (cm^{-1}): PA-dd-mea: 1729 (C=O stretching from the ester), 1229 (C-O-C stretching asymmetric), 1117 (C-H inplane bending mode 18a and 18b), 1033 (C-O-C stretching symmetric), 937 (C-H out-of-plane bending vibration bands oxazine mode 10a and trisubstituted benzene). PA-DD-Apa: 1725 (C=O stretching from the ester), 1227 (C-O-C stretching asymmetric), 1171 (C-H inplane bending mode 18a and 18b), 1043 (C-O-C stretching symmetric), 946 (C-H out-of-plane bending vibration bands oxazine mode 10a and trisubstituted benzene). PA-EG-mea: 1730 (C=O stretching from the ester), 1231 (C-O-C stretching asymmetric), 1143 (C-H inplane bending mode 18a and 18b), 1049 (C-O-C stretching symmetric), 934 (C-H out-of-plane bending vibration bands oxazine mode 10a and trisubstituted benzene). PA-EG-Apa: 1727 (C=O stretching from the ester), 1226 (C-O-C stretching asymmetric), 1155 (C-H inplane bending mode 18a and 18b), 1043 (C-O-C stretching symmetric), 943 (C-H out-of-plane bending vibration bands oxazine mode 10a and trisubstituted benzene).

2.1.4. Curing of Benzoxazine Thermoset

All monomers were poured into square Teflon molds (5/5/0.1 cm), then degassed under pressure in an oven at 100 °C (15 min). Afterward, samples were heated at 160 °C for 120 min to obtain the corresponding polymerized products: pPA-DD-mea, pPA-DD-Apa, pPA-EG-mea, and pPA-EG-Apa. FTIR (cm^{-1}) pPA-DD-mea:1729 (C=O stretching from the ester), 876 (out-of-plane, out-of-phase hydrogen wagging node for the 1,2,3,5-tetrasubstituted aromatic ring). pPA-DD-Apa: 1725 (C=O stretching from the ester), 872 (out-of-plane, out-of-phase hydrogen wagging node for the 1,2,3,5-tetrasubstituted aromatic ring). pPA-EG-mea: 1729 (C=O stretching from the ester), 873 (out-of-plane, out-of-phase

hydrogen wagging node for the 1,2,3,5-tetrasubstituted aromatic ring). pPA-EG-Apa: 1728 (C=O stretching from the ester), 872 (out-of-plane, out-of-phase hydrogen wagging node for the 1,2,3,5-tetrasubstituted aromatic ring).

2.1.5. Coating Preparation

AA1050 substrates with dimensions of 50 mm × 50 mm × 1.0 mm and chemical compositions of (weight percent) <0.40% Fe, <0.25% Si, <0.07% Zn, <0.05% Cu, <0.05% Mg, <0.05% Ti, and <0.05% Mn balanced with Al [11] were first etched with NaOH 1 M solution at 60 °C for 2 min and with nitric acid for 1 min after being rinsed with deionized water. These substrates were further washed with deionized water and dried in air.

PA samples were applied on the Al substrates by solvent casting in a 112.5 g/L chloroform solution at 45 °C. All samples were then heated at 160 °C for 120 min to obtain the corresponding polymerized coatings. The thickness of coatings was 100 ± 5 µm, which was measured using a dualscope MP0.

2.2. Characterization

2.2.1. Chemical and Morphological Characterization

The experimental procedure involved the recording of Fourier transform infrared (FTIR) spectra. This was achieved through the utilisation of a Fourier transform tensor 27 spectrometer 600–4000 cm^{-1} (Brüker, Ettlingen, Germany). This instrument boasts a resolution of 2 cm^{-1} and an accumulation of 32 scans.

The nuclear magnetic resonance (NMR) experiment was carried out utilising a Bruker AVANCEII-500 spectrometer manufactured in Karlsruhe, Germany, at ambient temperature. The solvent used was dimethyl sulfoxide (DMSO).

Gel content (GC) testing was carried out in both water and dioxolane, with 0.3 g of the dry material (heated to 100–120 °C for 100–120 min) being immersed at ambient temperature in 25 mL of solvent for a 14 day period. The samples were then subjected to a drying process at 100 °C in an oven for a period of 24 h. The gel content was subsequently determined by employing Equation (1).

$$GC(\%) = \frac{m_i - m_d}{m_i} * 100 \quad (1)$$

In the following formula, m_i and m_d represent the initial and dried mass, respectively. The reported values are the average of three measurements.

Swelling ratio water/acid (W) tests were conducted in water and 0.1 M sulfuric acid by immersion at ambient temperature. A quantity of 0.3 g of the material was immersed in 25 mL of solvent for a period of 14 days. Subsequent to this, the samples were meticulously wiped clean and weighed. The swelling ratio of water was determined according to Equation (2).

$$W(\%) = \frac{m_i - m_s}{m_i} * 100 \quad (2)$$

The variables m_i and m_s represent, respectively, the initial mass and the swollen mass at a given time. The reported values represent an average of three measurements.

2.2.2. Surface Wettability Test

The measurement of contact angles was conducted utilising a DSA 10 Mk2 drop shape analysis system (Krüss, Hamburg, Germany). The experiment was configured as a three-phase system, encompassing the coating surface, air, and a water drop. Specifically, 5 µL of water was dispensed onto the surface of each coating, and images were captured at 2× magnification, under white light (5500 K).

2.2.3. Thermal Analyses

Thermogravimetric analysis (TGA) was conducted utilising a TGA Q50 TA Instruments (TA Instruments, Zellik, Belgium) apparatus. Approximately 10 milligrams of each sample was analysed, with a temperature ranging from 25 to 800 °C at a heating rate of 10 °C per minute. The analysis was conducted under nitrogen gas, with a flow rate of 60 millilitres per minute.

The differential scanning calorimetry (DSC) experimental data were collected via the Q1000 TA Instruments apparatus (TA Instruments, Zellik, Belgium), operating within an inert atmosphere (N2) and employing a linear heating ramp from −40 to 250 °C at 10 °C/min rate on a specimen weighing approximately 10 mg.

2.2.4. Mechanical and Thermo-Mechanical Properties

Dynamic rheological analysis (DRA) was conducted using a compact and modular MCR 302 instrument from Anton Paar, Graz, Austria. This instrument was equipped with a temperature control device, as well as a disposable aluminium plate configuration. The temperature ramp tests were performed using oscillatory mode at a frequency of 1 Hz at a strain level of 10% using a 2.5 mm diameter plate with a 1 mm gap.

The dynamic mechanical analysis (DMA) was performed using a DMA Q800 TA Instruments analyser (TA Instruments, Zellik, Belgium). For neat matrices, DMA was carried out on rectangular samples (40/13/1 mm) in tensile mode with an amplitude of 2 μm at a frequency of 1 Hz, and a heating rate of 3 °C/min from 25 to 200 °C. The crosslinking density (ν') was determined by applying Equation (3).

$$\nu_{E'} = \frac{E'_R}{3 * R * T_R} \quad (3)$$

In this equation, E'_R denotes the storage modulus at the rubber state (MPa), T_R represents the temperature at 60 °C above the glass transition temperature (Tg) (K), and R is the gas constant.

Stress relaxation tests were carried out on specimens that were identical in dimensions to those utilised for DMA tests. A constant 2% strain was applied for each test, and the relaxation modulus was obtained. The stress relaxation behavior was then studied at a range of temperatures between 150 and 180 °C. For each system under investigation, the test was performed on a representative specimen. The results obtained were fitted using a Maxwell model, according to Equation (4).

$$\tau^* = \tau e^{\frac{E_a}{RT}} \quad (4)$$

The parameters of this equation are as follows: T denotes the test temperature, τ signifies the characteristic relaxation time at infinite temperature, R denotes the universal gas constant, and E_a represents the activation energy of bond exchange reactions.

2.2.5. Electrochemical Measurements

The electrochemical impedance spectroscopy (EIS) measurements were performed in 0.1 M H_2SO_4 solution with a Parstat (Model 2273) equipment (Princeton Applied Research, Oak Ridge, TN, USA) controlled by Powersuit® software (version 2.60). A platinum counter electrode, an Ag/AgCl (sat. KCl) reference electrode, and coated Al alloy substrates, as working electrodes, were used for these measurements. EIS test was performed on a 7 cm^2 exposed area of coated samples (working electrode), in a frequency range from 100 kHz to 0.01 Hz with 60 points using a 30 mV peak-to-peak sinusoidal voltage. Experiments were carried out in a Faraday cage three times at room temperature (22 ± 2 °C).

2.2.6. Adherence Properties

The cross-cut adhesion test was carried out according to the ISO 2409 standard [42]. The coatings were incised by three parallel knives to produce a grid. An adhesive tape elcometer ISO 2409 and ISO 8502-3 [43] was applied for 30 s on the coating and quickly removed. The aspect of the coating was further analysed by microscopy and compared with the standard class.

3. Results and Discussion

3.1. Characterization and Curing Behavior of Benzoxazine Monomer

Two bi-functional esterified phenols were successfully synthesized in solvent-free conditions from biobased phloretic acid and decandiol/ethylene glycol in the presence of a catalytic amount of para-toluenesulfonic acid. Further purification was performed to remove the catalyst and unconverted diols. As shown in Figure 2, the ester's characteristic peaks appeared at 2.74 and 3.97 ppm, corresponding to the methylene protons adjacent to the carbonyl moieties β- and α-positions. The aromatic ring is associated with chemical shifts in the range of 6.65–7.00 ppm. Then, the monomer was synthesized by reacting the purified esters and paraformaldehyde with the aliphatic amine (monoethanolamine) and the aromatic amine (aminophenyl ethyl alcohol). The obtained monomers were PA-EG-mea, PA-EG-Apa, PA-DD-mea, and PA-DD-Apa. The chemical structures of the four benzoxazine resins based on phloretic acid were confirmed using 1H-NMR and FTIR spectroscopy. The benzoxazine ring proton resonance attributed to O-CH2-N and Ar-CH2-N appeared at 4.78 and 3.92 ppm for mea-based benzoxazine and 5.36 and 4.53 ppm for Apa-based benzoxazine, respectively. Furthermore, the disappearance of the phenolic peak at 9.18 ppm confirms the completion of the reaction. FTIR analyses were performed to verify the functional groups present in these benzoxazine resins based on phloretic acid. Spectra of all monomers can be found in SI (SI Figure S1). The sharp peak at 1727 cm^{-1} indicates the successful formation of the ester band. The FTIR spectrum showed characteristic oxazine ring absorbance at 934, 1229, 1116, and 1031 cm^{-1}, corresponding, respectively, to the out-of-plane bending of H-C-H, C-X stretching mode 13 + C-O-C aromatic asymmetric stretching, CH inplane bending mode 18a/b, and C-O-C stretching symmetric [44].

The polymerization behaviors of benzoxazine groups were monitored using FTIR, DSC, and rheological experiments. The results are presented in Figures 3 and 4, and Table 1, respectively.

Table 1. Thermal and rheological behavior of (a) PA-DD-mea, (b) PA-DD-Apa, (c) PA-EG-mea, and (d) PA-EG-Apa.

Samples	Onset Exotherm DSC (°C)	Max Exotherm DSC (°C)	Enthalpy (J/g)	Initial Curing Temperature (Rheology) (°C)	T5% TGA (°C)
PA-DD-mea	163	209	48.4	189	213
PA-DD-Apa	147	228	163.4	206	234
PA-EG-mea	129	170	45.2	154	243
PA-EG-Apa	147	212	188.0	184	236

The rheological analysis was used to track the polymerization progress. All monomers exhibited a decrease in complex viscosity until reaching a plateau of 0.1 Pa·s at approximately 50 °C. The presence of the aromatic ring in the PA-DD monomer is evident from the significant increase in complex viscosity at room temperature. The sharp increase in viscosity for all resins is attributed to the ring-opening polymerization (ROP) of the

benzoxazine moieties. The curing process for PA-EG-Apa and PA-DD-Apa was slowed down due to the higher aromatic content. As a result, the initial curing temperature, which corresponds to the onset of a sharp increase in viscosity, is lower in the presence of the aliphatic amine. Specifically, the temperature occurs at 154 and 189 °C for MEA-based resins compared to 184 and 206 °C for Apa-based monomers.

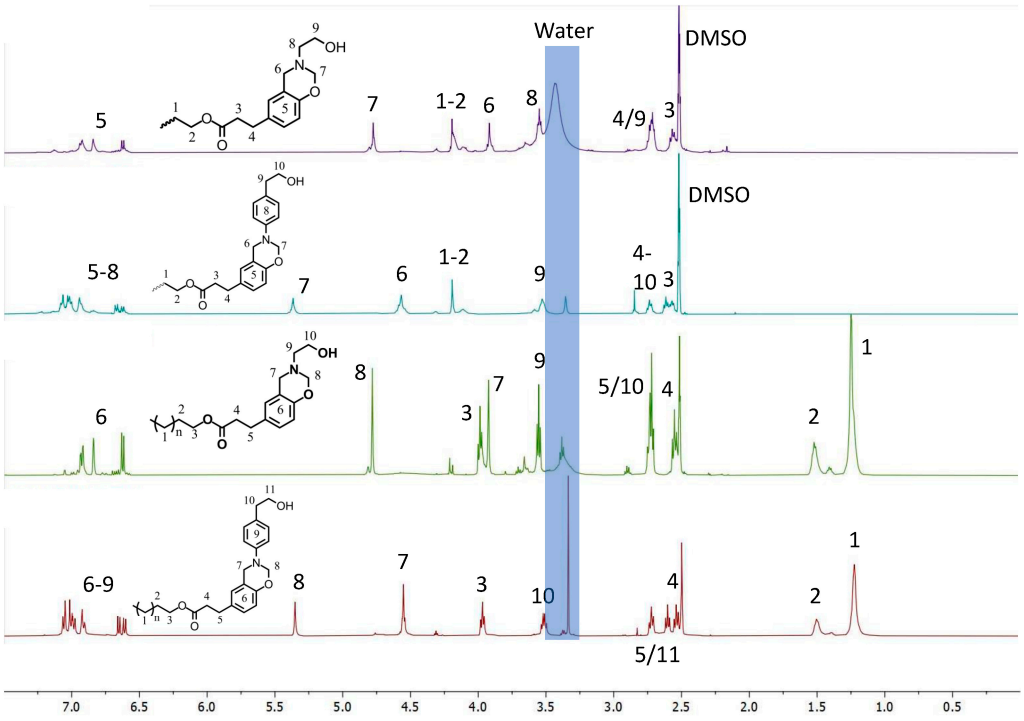

Figure 2. 1H-NMR spectra of PA-DD-mea, PA-DD-Apa, PA-EG-mea, and PA-EG-Apa.

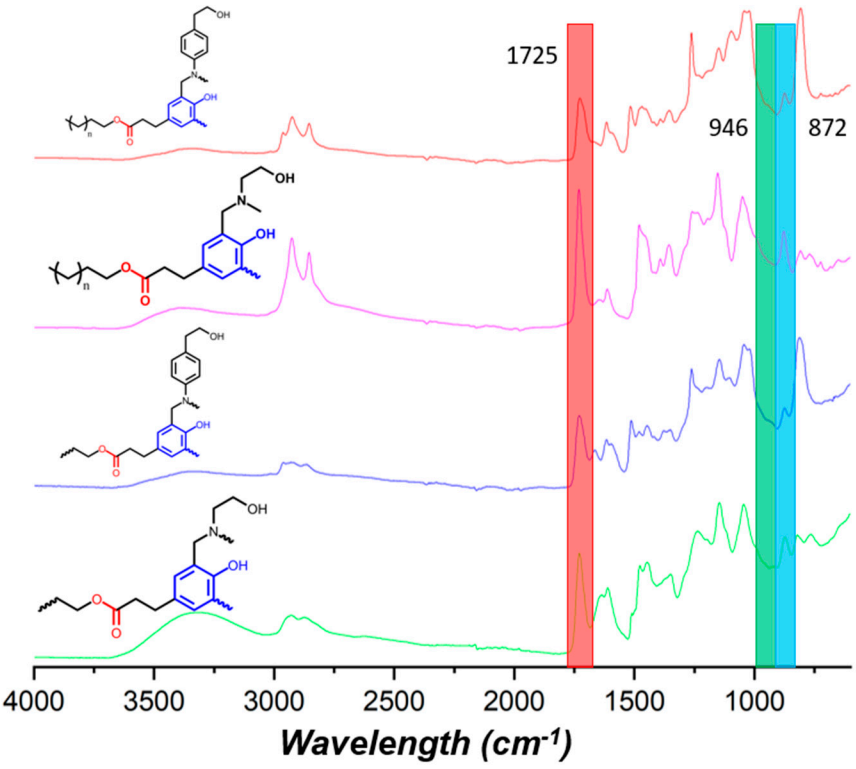

Figure 3. FTIR spectra of PolyPA-DD-mea, PolyPA-DD-Apa, PolyPA-EG-mea, and Poly-EG-Apa.

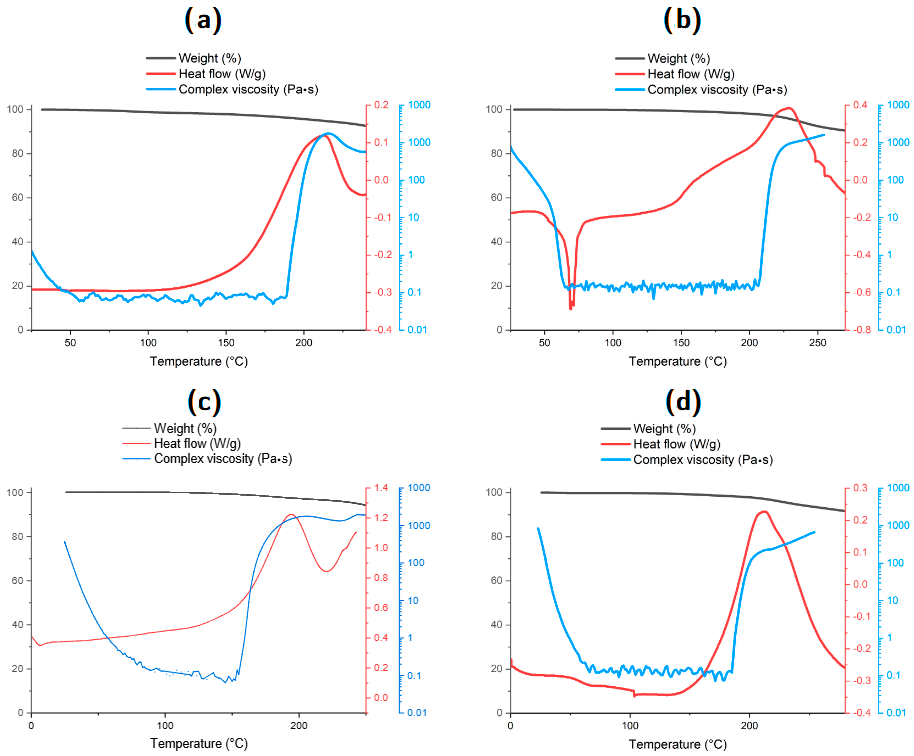

Figure 4. DSC, TGA, and rheological behavior of (**a**) PA-DD-mea, (**b**) PA-DD-Apa, (**c**) PA-EG-mea, and (**d**) PA-EG-Apa.

The DSC thermograms show that PA-EG-mea has two distinct exothermic peaks, which distinguishes it from PA-DD-mea and Apa-based monomers. The first peak at 170 °C corresponds to the ring-opening polymerization of the resin, while the second peak is associated with the degradation of the monomer, as confirmed by TGA analysis. However, in the case of the other three systems, these two exotherms are combined, which makes it difficult to accurately measure the enthalpy. This is probably due to the lower temperature resistance of PA-DD-mea and the higher energies needed for the polymerization of the system in Apa-based resins, as indicated by rheological analysis. Furthermore, the maximum exothermic peak shifts to a higher value (170 to 212 °C for the PA-EG systems) when an aromatic amine is used, which is consistent with the DSC results. This finding is in line with previous research by Dogan et al., who demonstrated that the presence of aromatics tends to increase the polymerization temperature [45]. Additionally, the catalytic effect of the free hydroxyl group held by the two amines is demonstrated. Kudoh et al. explained this high reactivity, which is provided by the neighboring group participation of the hydroxyl group through intramolecular reaction with cationic moieties of the zwitterionic intermediates formed by the ring-opening reaction of benzoxazine [46].

The polybenzoxazine network formation is confirmed by the typical band of the out-of-phase hydrogen wagging node for the 1,2,3,5-tetrasubstituted aromatic ring at 872 cm^{-1} (Figure 3) observed through FTIR. Additionally, the opening of benzoxazine cycles is certified by the disappearance of the characteristic peaks of benzoxazine at 934 and 1229 cm^{-1}.

These characteristics have confirmed the successful formation of a polybenzoxazine network.

3.2. Properties of Benzoxazine Polymers

The completeness of cross-linked polymer formation was certified using gel content tests. The incorporation of aromatic amine into the network increases the soluble fraction within the macromolecule. This may be due to easier solvent penetration into the network

resulting from the higher free volume fraction induced by steric hindrance of the aromatic amine. The gel content of the PA-EG and PA-DD systems decreased by 7% (Table 2).

Table 2. Properties of PA-DD-mea, PA-DD-Apa, PA-EG-mea, and PA-EG-Apa polymers.

Samples	Storage Modulus at RT (MPa)	Tg DMA (°C)	Storage Modulus in Rubber State (MPa)	Crosslinking Density (mol/L)	T5% (°C)	Char Yield (%)	Gel Content (%)	Swelling Ratio in Water (%)	Swelling Ratio in Acid (%)
pPA-DD-mea	770	57	8.4	0.9	255	23	95.7 ± 0.5	3.2 ± 0.2	53.0 ± 0.2
pPA-DD-Apa	2100	93	6.3	0.6	311	27	88.8 ± 1.2	1.6 ± 0.1	3.8 ± 0.1
pPA-EG-mea	1850	127	20.6	1.8	241	35	98.7 ± 0.5	6.2 ± 0.2	58.0 ± 0.5
pPA-EG-Apa	3110	103	2.4	0.2	292	37	91.6 ± 0.4	2.3 ± 0.1	2.7 ± 0.2

The thermo-mechanical properties and relaxation behavior of the polybenzoxazine network were analysed using TGA and DMA experiments, respectively, to evaluate the effect of the aromatic ring directly linked to the tertiary amine. All of the results can be found in Figure 5 and in Table 2.

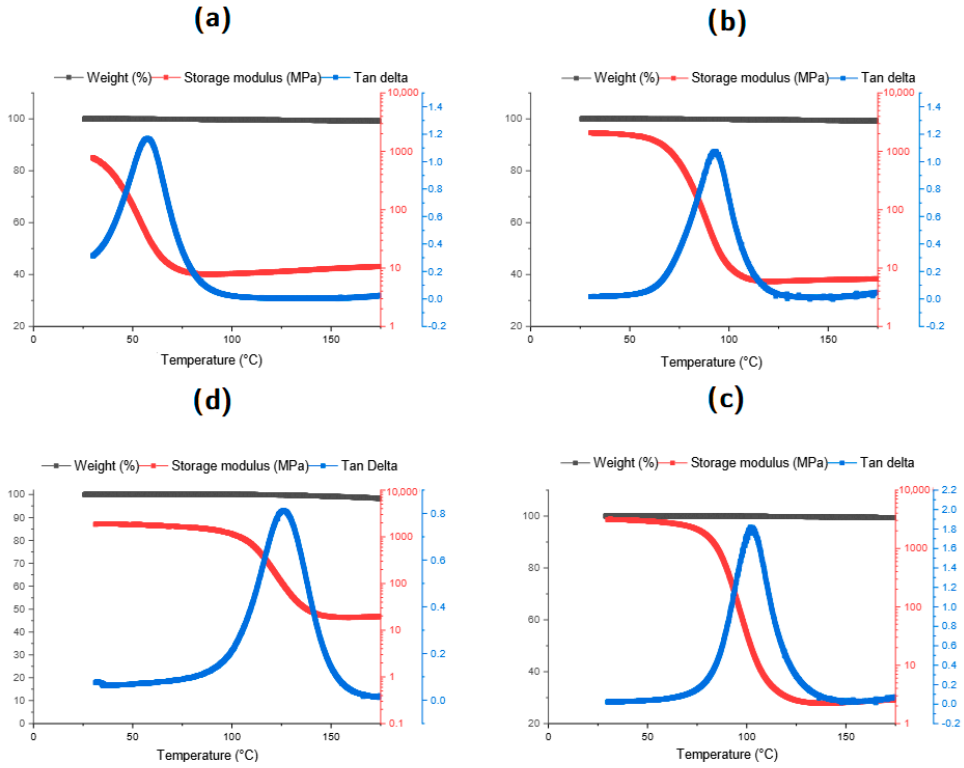

Figure 5. DMA and TGA behavior of (**a**) pPA-DD-mea, (**b**) pPA-DD-Apa, (**c**) pPA-EG-mea, and (**d**) pPA-EG-Apa.

Thermogravimetric analysis was used to study the thermal stability of polymerized samples. It can be observed in Table 2 that the thermal stability of the macromolecule increases with a higher content of aromatic rings. In this sense, pPA-DD-Apa and pPA-EG-Apa showed better thermal behavior with T5% around 311 and 292 °C compared to the aliphatic system around 255 and 241 °C, respectively. The same behavior is highlighted with the char yield. Moreover, a stiffer material can be obtained due to the presence of aminophenyl ethyl alcohol in the system. In a certain way, pPA-DD-Apa and pPA-EG-Apa showed higher storage moduli at room temperature (2100 and 3110 MPa, respectively) compared to the monoethanolamine network (770 and 1850 MPa, respectively). Conversely, the addition of the benzene ring tends to decrease the cross-linking density (from 1.8 to 0.2 for the pPA-EG network), which is consistent with the gel content measurement. The

low Apa values could be explained by the conformation of these macromolecules induced by the higher aromatic content. Therefore, the structure of these polymers would be more favorable for interactions by hydrogen bridges $\pi-\pi$ stacking and fewer covalent bonds, which could explain the drop in mechanical properties at higher temperatures.

Interestingly, the evolution of the glass temperature does not strictly follow this trend. While the pPA-DD-Apa system shows a positive Tg evolution (57 to 93 °C), the pPA-EG-Apa network shows a decrease (127 to 103 °C). The Tg variation can be explained by several different structural features, such as crosslink density, steric hindrance, and chain stiffness, which affect the Tg of a thermoset. On the one hand, a configuration more favorable to hydrogen bridging $\pi-\pi$ stacking may increase the glass transition temperature. On the other hand, steric hindrance caused by the addition of an aromatic ring can lead to a decrease in Tg.

Finally, as expected, the hydrophobic and anti-protonation behavior of the Apa-based system increases as compared with mea networks. For example, the water swelling rate of the EG-based macromolecule decreases from 6.2 to 2.3% after 14 days of immersion at room temperature, while the presence of the aromatic ring on the tertiary amine provided less acid absorption (from 58.0 to 2.7% for EG-based systems).

3.3. Relaxation of Benzoxazine Systems

The dynamic properties of polybenzoxazine resins were studied by a stress relaxation test performed by DMA in tensile mode applying 2 µm of amplitude at a frequency of 1 Hz at a higher temperature than Tg's polymers. Figure 6 and Table 3 show the results of the normalized stress relaxation E/E0 as a function of time from 130 to 160 °C.

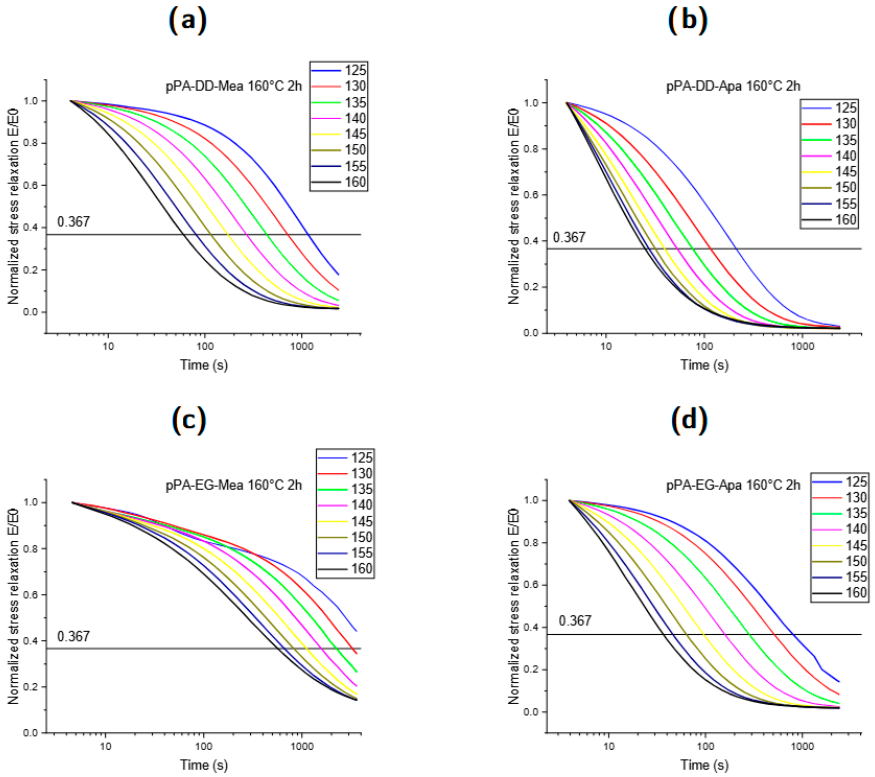

Figure 6. Normalized stress relaxation curve of (**a**) pPA-DD-mea, (**b**) pPA-DD-Apa, (**c**) pPA-EG-mea, and (**d**) pPA-EG-Apa.

Table 3. Relaxation time of polybenzoxazine network.

Temperature (°C)	Relaxation Time of pPA-DD-mea (s)	Relaxation Time of pPA-DD-Apa (s)	Relaxation Time of pPA-EG-mea (s)	Relaxation Time of pPA-EG-Apa (s)
130	605	117	3103	517
135	382	75	2335	284
140	258	53	1646	160
145	170	39	1185	96
150	117	32	873	64
155	84	28	686	46
160	65	25	589	37

Thanks to the Maxwell model for viscoelastic fluids, which is typically employed in the context of covalent adaptive networks based on the transesterification mechanism, the characteristic relaxation time (T), defined as the time corresponding to 1/e of E(t)/E0, was obtained for each temperature and the activation energies were calculated following Arrhenius' law (Table 4). For example, (T) at 150 °C, corresponding to the relaxation time at 150 °C, was 117, 32, 873 and 64 s for pPA-DD-mea, pPA-DD-Apa, pPA-EG-mea, and pPA-EG-Apa, respectively. The likely free volume provided by the aromatic amine allows fast transesterification reactions between the ester moieties and the free hydroxyl group carried by the primary amine [47]. Moreover, the low relaxation time obtained for all of the systems could be explained by the abundance of tertiary amine in the network, which may favor the nucleophilic substitution of the ester [38].

Table 4. Transesterification activation energies of each polybenzoxazine network.

Samples	R^2 Ln Tau	Ea Ln Tau (kJ/mol)
pPA-DD-mea	0.9989	113.6
pPA-DD-Apa	0.9845	92.3
pPA-EG-mea	0.9994	96.2
pPA-EG-Apa	0.9917	140.3

The Arrhenius relation of ln (π) versus 1000/T for all systems is shown in Figure 7. According to the Arrhenius equation, the activation energies were calculated by multiplying the perfect gas constant with the slope of the obtained line. Surprisingly, the incorporation of an aromatic amine does not have the same effect on both networks. While its presence generally lowers the minimum energy required to initiate transesterification in polymers synthesized from decandiol (from 113.6 to 92.3 kJ/mol), it appears to have the opposite effect in the ethylene glycol system, i.e., an increase in the required energy (from 96.2 to 140.3 kJ/mol). Nevertheless, the calculated values are consistent with dynamic covalent bonding mechanisms, especially in the area of transesterification internally catalyzed by tertiary amine [38,48,49].

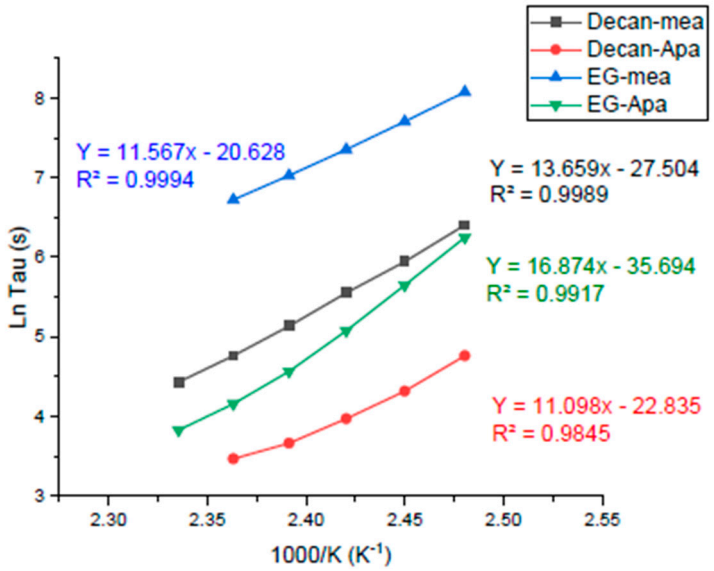

Figure 7. Arrhenius fits of all networks.

3.4. Adhesion of Polybenzoxazine Coatings

Optimal adherence of all polybenzoxazines onto the metallic substrate was demonstrated using the cross-cut adhesion test following the ISO 2409 standard. Figure 8 shows the 5B rating of all systems with any coating detachment and intact edges after the use of the adhesive.

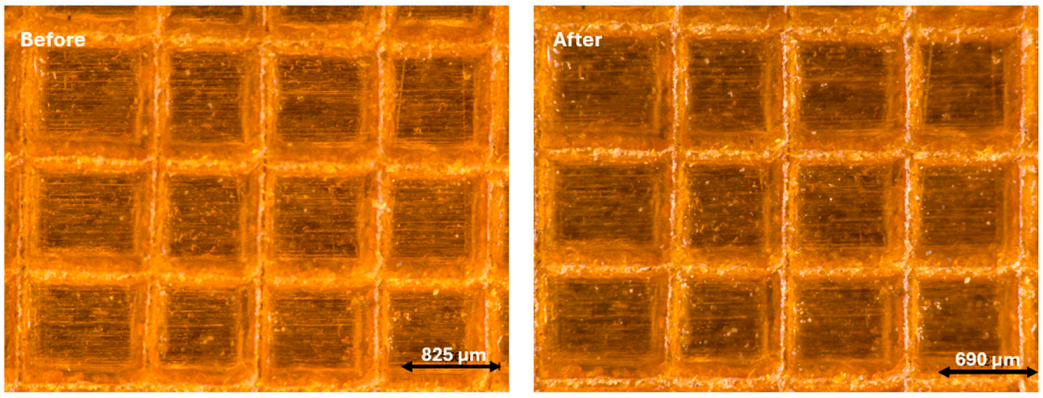

Figure 8. Cross-cut adhesion test of pPA-DD-Apa.

3.5. Acid Resistance of Polybenzoxazine Coatings on A1050 Al Alloy

EIS measurements were performed in 0.1 M H_2SO_4 solution for acid resistance analysis of polybenzoxazine coatings. Figure 9 shows the Bode plots of blank Al substrates (without coating) after 14 days of immersion time. After 1 day, the impedance modulus at the low frequency of 0.01 Hz, as the representative of the whole system resistance [50], decreased from 1370 to 392 $\Omega \cdot cm^2$. There is a capacitive loop at middle frequency, which is attributed to the charge-transfer process and interfacial reactions due to the oxidation of Al and reduction of water [51]. Moreover, the inductive loop at low frequency can be associated with the surface relaxation of intermediate species, as well as the adsorption of H^+ and SO_4^{2-} ions on the surface.

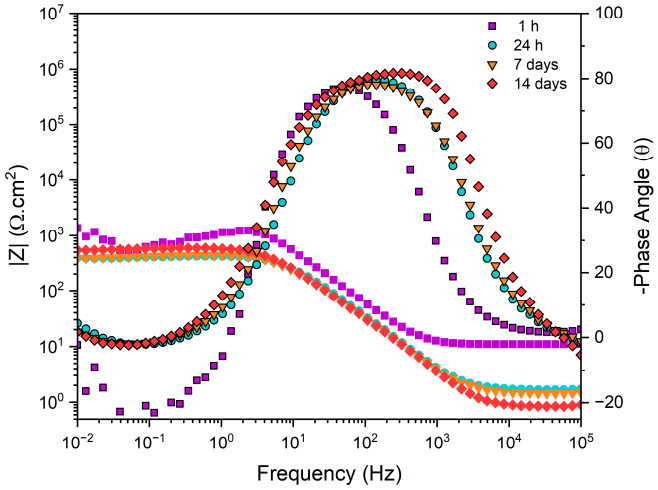

Figure 9. Bode plots of blank Al alloy substrate in 0.1 M H_2SO_4 solution.

The Bode plots of samples with polybenzoxazine coatings at various immersion times are presented in Figure 10. The impedance modulus at low frequency, as indicated by the graphs, exhibits a notably higher value for the Apa coating in comparison to the mea coating. The DD-Apa coating demonstrates superior corrosion resistance performance, maintaining adequate protection after 14 days of immersion, with the impedance modulus value of 1.8×10^7 Ω·cm^2 at 0.01 Hz frequency. However, both DD-mea and EG-mea coatings display failure after 7 and 1 day of immersion, respectively.

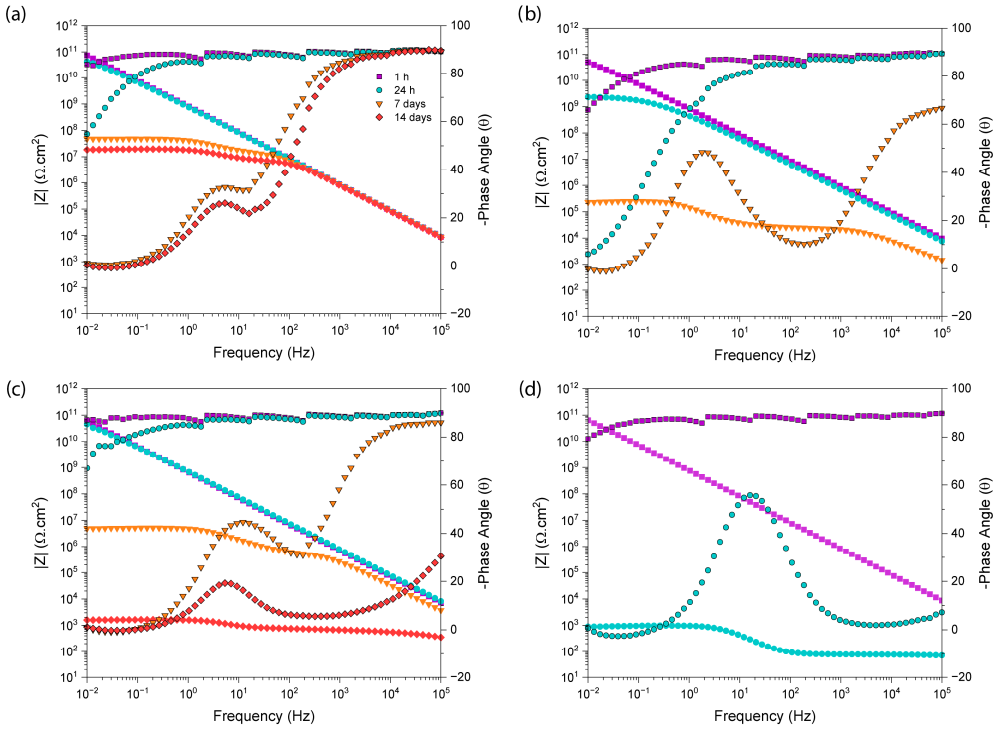

Figure 10. Bode plots of (**a**) pPA-DD-Apa, (**b**) pPA-DD-mea, (**c**) pPA-EG-Apa, and (**d**) pPA-EG-mea coated, after immersion in 0.1 M H_2SO_4 solution.

The assessment of Bode phase diagrams at high frequencies for the samples reveals proper barrier properties of the DD-Apa coating after 14 days, evidenced by a phase angle at approximately −90° [15]. However, after 1, 7, and 14 days of immersion for EG-mea, DD-mea, and EG-Apa coatings, respectively, a reduction in phase angle at high frequency

was observed, coupled with the emergence of a time constant within the middle-frequency range (100–10^2 Hz), indicative of a loss in coating protection.

The electrical equivalent circuits (EECs) depicted in Figure 11 were employed to fit the EIS diagrams and for a better visual representation, Figure 12a illustrates the impedance modulus of the samples at low frequency versus immersion time.

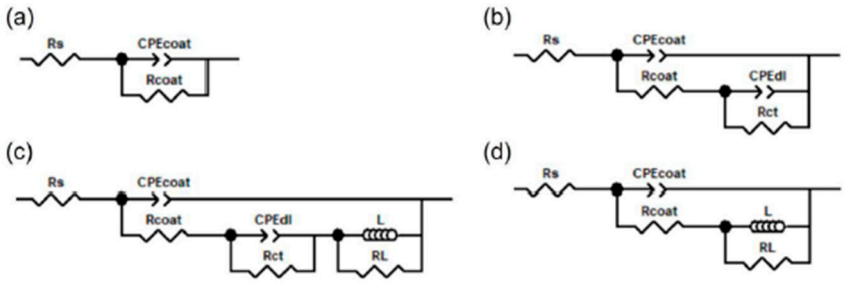

Figure 11. Electrical equivalent circuits (EEC) for fitting EIS data of (**a**) DD-Apa and EG-Apa coatings after 1 day immersion, (**b**) DD-Apa after 7 and 14 days and DD-mea after 1 day immersion, (**c**) DD-mea after 7 day immersion and EG-Apa after 7 and 14 days of immersion, (**d**) EG-mea after 1 day immersion, on Al substrates.

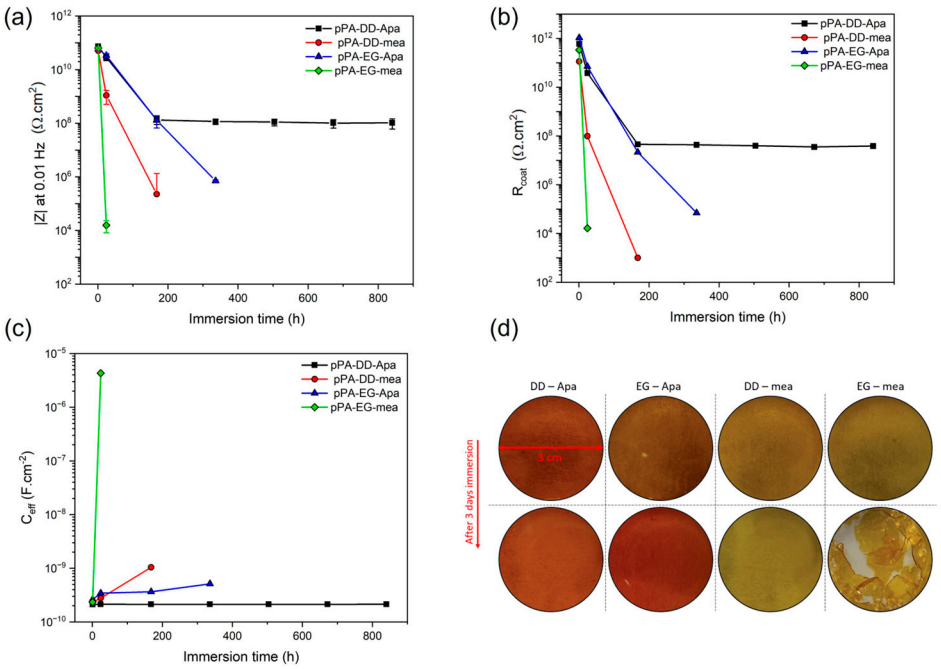

Figure 12. (**a**) The impedance at low frequency (|Z|), (**b**) pore resistance of coatings (R*coat*), and (**c**) effective capacitance (C*eff*), obtained from fitting EIS data after immersion in 0.1 M H_2SO_4 solution. (**d**) Macroscopic images of the coatings' surface after immersion in 0.1 M H_2SO_4 solution for 3 days.

For the fitting of DD-Apa coating during a 1 day immersion period, the EEC shown in Figure 11a was utilised, wherein CPE*coat* and R*coat* represent the constant phase element and pore resistance of the coatings, respectively. In Figure 12b, it can be observed that the resistance of the coatings (R*coat*) was decreased over time, which is attributed to the electrolyte's diffusion within the coatings [52]. However, the smallest decrease can be found in DD-Apa coating after 14 days of immersion. After 7 days, another capacitive loop emerged, indicative of the Al oxidation and the charge-transfer process (Figure 11b). EEC in Figure 11b was used for the EIS data fitting of DD-Apa for immersion times after 7 days, in which R*ct* and CPE*dl* are the charge-transfer resistance and the double layer capacitance,

respectively. For DD-mea coatings, Figure 11b was employed for fitting the EIS data after 1 day of immersion. However, for the 7 day immersion period, an inductive loop was added to the EEC, as illustrated in Figure 11c, denoted by L and R*L*, representing the inductance and resistance of inductance, respectively. In the case of sample EG-Apa, Figure 11a was initially used for fitting EIS data after 1 h and 1 day of immersion. Subsequently, for 7 and 14 days of immersion, with the appearance of a middle-frequency loop and an inductive loop, Figure 11c was adopted. For sample EG-mea, exhibiting the lowest acid resistance, Figure 11a,d were applied for fitting EIS data during the 1 h and 1 day immersion periods.

Due to the non-ideal behavior of capacitors, effective capacitance (C_{eff}) can be determined using CPE obtained from the fitting of EIS data [53]. The equation Hsu and Mansfeld (Equation (5)) can be used for this purpose (n is the constant phase element parameter) [54]. C_{eff} can be also related to the physical properties of the coating using Equation (6), in which ε_0, ε, and d correspond to the permittivity of vacuum, the dielectric constant, and thickness of the coating, respectively.

$$C_{eff} = \mathrm{C} \cdot \mathrm{P} \cdot E_{coat}^{\frac{1}{n}} \cdot R_{coat}^{\frac{(1-n)}{n}} \quad (5)$$

$$C_{eff} = \frac{\varepsilon_0 \cdot \varepsilon}{d} \quad (6)$$

With passing time, C_{eff} of the coatings increases, which can be due to the absorption of electrolyte and an increase in the effective dielectric constant (ε), as the dielectric constant of water, present in the acid solution, is higher than polymers and there is a direct correlation between ε and C_{eff} (Equation (6)) [53]. The graphical representation of C_{eff} over immersion time is provided in Figure 12c. As can be seen, C_{eff} increased at a higher rate for samples with mea and, more specifically, EG-mea followed by EG-Apa and DD-Apa, respectively. These results align with the swelling ratio results of samples in H_2SO_4, which shows a higher swelling ratio for EG-mea and DD-mea (Table 2). Moreover, the hydrophobic and anti-protonation of APa-based coatings resulted in better acid resistance behavior. Diffusion of species in the coating and the swelling can promote electrolyte contact with the Al alloy substrate, leading to the loss of mechanical properties (physical degradation), as well as corrosion resistance (chemical and electrochemical degradation) [52].

The performance of the coatings can be also assessed by visual observations in the search for delamination, blistering, cracks, and/or color change [52]. Figure 12d represents macroscopic images of the coatings immersed in 0.1 M H_2SO_4 for 3 days. DD coatings, regardless of Apa or mea, did not exhibit significant alterations in color and physical appearance. However, EG coatings demonstrated changes in their visual characteristics, including delamination in EG-mea coating and a shift in color from light to dark orange in EG-Apa (Figure 12d).

4. Conclusions

The present study aimed to enhance the acid resistance and healing capacity of two mea-based polybenzoxazine resins, which feature a covalent adaptive network based on transesterification chemistry. The objective was achieved by the direct incorporation of an aromatic group linked to the tertiary amines, which are intrinsic to the system backbone. This approach limits the protonation of these amines through steric hindrance and/or mesomeric effects. For that, Apa-based polybenzoxazines resins were synthesized by replacing alkyl mea with aromatic Apa. The thermal and thermo-mechanical properties of all of the resulting systems were analysed using TGA/DSC/DMA. It seems that the presence of aromatic groups in the vicinity of the tertiary amines results in a notable enhancement of both the thermal and thermomechanical properties of the resins. This is evidenced by a considerable increase in T5% (255 to 311 °C), char yield (23 to 27%), storage modulus at room temperature (770 to 2100 MPa), and glass temperature (57 to

93 °C). Despite a reduction in gel content and cross-linking density, the incorporation of Apa into the decandiol benzoxazine system has been observed to result in the most notable enhancement in thermal and thermomechanical properties, as well as swelling characteristics. Furthermore, both the Apa systems demonstrated a notable reduction in the characteristic relaxation time (605 to 117 s at 130 °C), indicative of enhanced healing capacity, in comparison to the homologous mea systems. This could be explained by an increase in mobility induced by a higher free volume fraction with respect to the crosslinking density. Finally, the acid resistance of all the polybenzoxazines systems coated on etched AA1050 substrate was evaluated by EIS. Again, both Apa-based benzoxazine systems showed the best behavior thanks to the presence of the aromatic ring directly linked to the tertiary amine, which can act as a barrier against protonation induced by acid species. The prevention of the plasticization of the system by the proton attacks onto the tertiary amine moieties induced by the presence of aromatic amine can be directly observed through the evolution of the coatings' aspects after three days of immersion in a 0.1 M H_2SO_4 solution. Among the Apa-based systems, the best protection was found for the polybenzoxazine network synthesized with decandiol, a long aliphatic diol, which, thanks to its higher hydrophobic properties, shows good corrosion in sulfuric acid media even after 35 days of immersion.

Supplementary Materials: The following supporting information can be downloaded at: https://www.mdpi.com/article/10.3390/coatings15010067/s1, Figure S1: H NMR spectra of PA-DD-mea, PA-DD-Apa, PA-EG-mea and PA-EG-Apa.

Author Contributions: Conceptualization, methodology, investigation, formal analysis, data curation, writing—original draft preparation, L.V.R. and R.M.; validation, supervision, funding acquisition, resources, writing—review and editing, L.B., M.-G.O. and J.-M.R.; Project administration, J.-M.R. All authors have read and agreed to the published version of the manuscript.

Funding: This research was funded by the Concerted Research Action in universities, an institutional funding for public research from Wallonia-Brussels Federation in the frame of ARC 2020–PROCOMAG project.

Institutional Review Board Statement: Not applicable.

Informed Consent Statement: Not applicable.

Data Availability Statement: The data that support the findings of this study are available from the corresponding authors upon reasonable request.

Acknowledgments: The authors wish to thank the Wallonia-Brussels Federation, Wallonia, and the European Community for general support in the frame of the Concerted Research Action program (ARC 2020–PROCOMAG project). L.B. also wants to thank HORIZON-JU-CBE-2023-R-04 for Project 101157517–SSUCHY-Next. JMR is FRS-FNRS senior research associate and a WEL-T principal investigator from FNRS under the CONSOLID program.

Conflicts of Interest: The authors declare no conflicts of interest.

References

1. Li, S.; Yue, X.; Li, Q.; Peng, H.; Dong, B.; Liu, T.; Yang, H.; Fan, J.; Shu, S.; Qiu, F.; et al. Development and applications of aluminum alloys for aerospace industry. *J. Mater. Res. Technol.* **2023**, *27*, 944–983. [CrossRef]
2. Gamin, Y.; Akopyan, T.; Koshmin, A.; Dolbachev, A.; Aleshchenko, A.; Galkin, S.P.; Romantsev, B.A. Investigation of the microstructure evolution and properties of A1050 aluminum alloy during radial-shear rolling using FEM analysis. *Int. J. Adv. Manuf. Technol.* **2020**, *108*, 695–704. [CrossRef]
3. Renaud, A.; Paint, Y.; Lanzutti, A.; Bonnaud, L.; Fedrizzi, L.; Dubois, P.; Poorteman, M.; Olivier, M.-G. Sealing porous anodic layers on AA2024-T3 with a low viscosity benzoxazine resin for corrosion protection in aeronautical applications. *RSC Adv.* **2019**, *9*, 16819–16830. [CrossRef] [PubMed]

4. Hosseiny, N.; Shabani, A.; Toroghinejad, M.R. Effect of bimodal microstructure on texture evolution and mechanical properties of 1050 Al alloy processed through severe plastic deformation and subsequent annealing. *Mater. Sci. Eng. A* **2021**, *820*, 141580. [CrossRef]
5. Fabris, R.; Masi, G.; Bignozzi, M.C. Corrosion Behavior of Aluminum Alloys in Different Alkaline Environments: Effect of Alloying Elements and Anodization Treatments. *Coatings* **2024**, *14*, 240. [CrossRef]
6. Kwolek, P. Corrosion behaviour of 7075 aluminium alloy in acidic solution. *RSC Adv.* **2020**, *10*, 26078–26089. [CrossRef]
7. Costa, M.; Klein, C.B. Toxicity and Carcinogenicity of Chromium Compounds in Humans. *Crit. Rev. Toxicol.* **2006**, *36*, 155–163. [CrossRef] [PubMed]
8. Weiner, M.; Salminen, W.; Larson, P.; Barter, R.; Kranetz, J.; Simon, G. Toxicological review of inorganic phosphates. *Food Chem. Toxicol.* **2001**, *39*, 759–786. [CrossRef]
9. Choong, T.S.; Chuah, T.; Robiah, Y.; Koay, F.G.; Azni, I. Arsenic toxicity, health hazards and removal techniques from water: An overview. *Desalination* **2007**, *217*, 139–166. [CrossRef]
10. Hu, R.-G.; Zhang, S.; Bu, J.-F.; Lin, C.-J.; Song, G.-L. Recent progress in corrosion protection of magnesium alloys by organic coatings. *Prog. Org. Coat.* **2011**, *73*, 129–141. [CrossRef]
11. Renaud, A.; Bonnaud, L.; Dumas, L.; Zhang, T.; Paint, Y.; Fasano, F.; Kulyk, O.; Pospisilova, E.; Nysten, B.; Delcorte, A.; et al. A ben-zoxazine/substituted borazine composite coating: A new resin for improving the corrosion resistance of the pristine benzoxa-zine coating applied on aluminum. *Eur. Polym. J.* **2018**, *109*, 460–472. [CrossRef]
12. Renaud, A.; Poorteman, M.; Escobar, J.; Dumas, L.; Paint, Y.; Bonnaud, L.; Dubois, P.; Olivier, M.-R.-G. A new corrosion protection approach for aeronautical applications combining a Phe-nol-paraPhenyleneDiAmine benzoxazine resin applied on sulfo-tartaric anodized aluminum. *Prog. Org. Coat.* **2017**, *112*, 278–287. [CrossRef]
13. Akande, I.G.; Fayomi, O.S.I.; Oluwole, O.O. Anticorrosion Potential of Inhibitive Suphtrim Drug on Aluminium Alloys in 0.5 M H_2SO_4. *J. Bio-Tribo-Corros.* **2020**, *6*, 1–8. [CrossRef]
14. Desai, P.; Desai, F.; Patel, A.; Parmar, B. Anticorrosive properties of Eucalyptus (Nilgiris) leaves extract on 2S grade aluminium in acid solutions. *Appl. Surf. Sci. Adv.* **2023**, *16*, 100414. [CrossRef]
15. Nardeli, J.V.; Fugivara, C.S.; Taryba, M.; Montemor, M.; Benedetti, A.V. Self-healing ability based on hydrogen bonds in organic coatings for corrosion protection of AA1200. *Corros. Sci.* **2020**, *177*, 108984. [CrossRef]
16. Dagdag, O.; Berisha, A.; Mehmeti, V.; Haldhar, R.; Berdimurodov, E.; Hamed, O.; Jodeh, S.; Lgaz, H.; Sherif, E.-S.M.; Ebenso, E.E. Epoxy coating as effective anti-corrosive polymeric material for aluminum alloys: Formulation, electrochemical and computational approaches. *J. Mol. Liq.* **2022**, *346*, 117886. [CrossRef]
17. Bandeira, R.M.; van Drunen, J.; Garcia, A.C.; Tremiliosi-Filho, G. Influence of the thickness and roughness of polyaniline coatings on corrosion protection of AA7075 aluminum alloy. *Electrochimica Acta* **2017**, *240*, 215–224. [CrossRef]
18. Contri, G.; Zimmermann, C.A.; Ramoa, S.D.A.D.S.; Schmitz, D.P.; Ecco, L.G.; Barra, G.M.d.O.; Fedel, M. Polypyrrole Modified E-Coat Paint for Corrosion Protection of Aluminum AA1200. *Front. Mater.* **2020**, *7*, 45. [CrossRef]
19. Lim, J.S.K.; Gan, C.L.; Hu, X.M. Unraveling the Mechanistic Origins of Epoxy Degradation in Acids. *ACS Omega* **2019**, *4*, 10799–10808. [CrossRef] [PubMed]
20. Anagwu, F.I.; Thakur, V.K.; Skordos, A.A. High-Performance Vitrimeric Benzoxazines for Sustainable Advanced Materials: Design, Synthesis, and Applications. *Macromol. Mater. Eng.* **2023**, *4*, 308. [CrossRef]
21. Poorteman, M.; Renaud, A.; Escobar, J.; Dumas, L.; Bonnaud, L.; Dubois, P.; Olivier, M.-G. Thermal curing of para -phenylenediamine benzoxazine for barrier coating applications on 1050 aluminum alloys. *Prog. Org. Coat.* **2016**, *97*, 99–109. [CrossRef]
22. Kiskan, B. Adapting benzoxazine chemistry for unconventional applications. *React. Funct. Polym.* **2018**, *129*, 76–88. [CrossRef]
23. Adjaoud, A.; Puchot, L.; Verge, P. Polybenzoxazine-based covalent adaptable networks: A mini-review. *Polymer* **2023**, *287*, 126426. [CrossRef]
24. Malekkhouyan, R.; Van Renterghem, L.; Bonnaud, L.; Paint, Y.; Gonon, M.; Cornil, D.; Cornil, J.; Raquez, J.M.; Olivier, M.G. Effect of surface pretreatment on the production of LDH for post-treatment with ben-zoxazine resin. *Surf. Coat. Technol.* **2024**, *479*, 130538. [CrossRef]
25. Klfout, H.A.; Asiri, A.M.; Alamry, K.A.; Hussein, M.A. Recent advances in bio-based polyben-zoxazines as an interesting adhesive coating. *RSC Adv.* **2023**, *13*, 19817–19835. [CrossRef] [PubMed]
26. Ishida, H. Chapter 1. In *Handbook of Benzoxazine Resins*; Ishida, H., Agag, T., Eds.; Elsevier: Amsterdam, The Netherlands, 2011.
27. Suesuwan, A.; Suetrong, N.; Yaemphutchong, S.; Tiewlamsam, I.; Chansaenpak, K.; Wannapaiboon, S.; Chuanopparat, N.; Srathongsian, L.; Kanjanaboos, P.; Chanthaset, N.; et al. Partially Bio-Based Benzoxazine Monomers Derived from Thymol: Photoluminescent Properties, Polymerization Characteristics, Hydrophobic Coating Investigations, and Anticorrosion Studies. *Polymers* **2024**, *16*, 1767. [CrossRef] [PubMed]
28. Deng, Y.; Xia, L.; Song, G.-L.; Zhao, Y.; Zhang, Y.; Xu, Y.; Zheng, D. Development of a cur-cumin-based antifouling and anticorrosion sustainable polybenzoxazine resin composite coating. *Compos. Part B Eng.* **2021**, *225*, 109263. [CrossRef]
29. Patil, D.M.; Phalak, G.A.; Mhaske, S.T. Synthesis and characterization of bio-based benzoxazine oligomer from cardanol for corrosion resistance application. *J. Coat. Technol. Res.* **2017**, *14*, 517–530. [CrossRef]

30. Appasamy, S.; Krishnasamy, B.; Muthukaruppan, A. Evaluation of optical, thermal and hydrophobic prop-erties of sustainable stilbene-based benzoxazines for high-performance utilization. *Mater. Chem. Phys.* **2024**, *329*, 130078. [CrossRef]
31. Adjaoud, A.; Puchot, L.; Federico, C.E.; Das, R.; Verge, P. Lignin-based benzoxazines: A tunable key-precursor for the design of hydrophobic coatings, fire resistant materials and catalyst-free vitrimers. *Chem. Eng. J.* **2022**, *453*, 139895. [CrossRef]
32. Bo, C.; Sha, Y.; Song, F.; Zhang, M.; Hu, L.; Jia, P.; Zhou, Y. Renewable benzoxazine-based thermosets from cashew nut: Investigating the self-healing, shape memory, recyclability and antibacterial activity. *J. Clean. Prod.* **2022**, *341*, 130898. [CrossRef]
33. Arslan, M.; Kiskan, B.; Yagci, Y. Recycling and Self-Healing of Polybenzoxazines with Dynamic Sulfide Linkages. *Sci. Rep.* **2017**, *7*, 1–11. [CrossRef] [PubMed]
34. Wang, X.; Zhang, S.; He, Y.; Guo, W.; Lu, Z. Reprocessable Polybenzoxazine Thermosets with High T_gs and Mechanical Strength Retentions Using Boronic Ester Bonds as Crosslinkages. *Polymers* **2022**, *14*, 2234. [CrossRef] [PubMed]
35. Wolf, A.; Pursche, L.; Boskamp, L.; Koschek, K. Amine Exchange of Aminoalkylated Phenols as Dynamic Reaction in Benzoxazine/Amine-Based Vitrimers. *Macromol. Rapid Commun.* **2024**, *45*, e2400557. [CrossRef]
36. Trejo-Machin, A.; Puchot, L.; Verge, P. A cardanol-based polybenzoxazine vitrimer: Recycling, reshaping and reversible adhesion. *Polym. Chem.* **2020**, *11*, 7026–7034. [CrossRef]
37. Van Renterghem, L.; Malekkhouyan, R.; Bonnaud, L.; Tavernier, R.; Olivier, M.; Raquez, J.-M. Solvent-free coatings based on bio-sourced benzoxazines resins with healing, repair, and recycling capabilities. *Prog. Org. Coat.* **2024**, *189*, 108316. [CrossRef]
38. Altuna, F.I.; Hoppe, C.E.; Williams, R.J. Epoxy vitrimers with a covalently bonded tertiary amine as catalyst of the transesterification reaction. *Eur. Polym. J.* **2019**, *113*, 297–304. [CrossRef]
39. Wang, M.W.; Jeng, R.J.; Lin, C.H. Study on the Ring-Opening Polymerization of Benzoxazine through Multisubstituted Polybenzoxazine Precursors. *Macromolecules* **2015**, *48*, 530–535. [CrossRef]
40. Arslan, M. Synthesis and characterization of novel bio-based benzoxazines from gallic acid with latent catalytic characteristics. *React. Funct. Polym.* **2019**, *139*, 9–16. [CrossRef]
41. Kim, H.-D.; Ishida, H. Study on the chemical stability of benzoxazine-based phenolic resins in carboxylic acids. *J. Appl. Polym. Sci.* **2000**, *79*, 1207–1219. [CrossRef]
42. *ISO 2409:2020*; Paints and varnishes—Cross-cut test. International Organization for Standardization: Geneva, Switzerland, 2020.
43. *ISO 8502-3:2017*; Preparation of steel substrates before application of paints and related products—Tests for the assessment of surface cleanliness—Part 3: Assessment of dust on steel surfaces prepared for painting (pressure-sensitive tape method). International Organization for Standardization: Geneva, Switzerland, 2017.
44. Dunkerst, J.; Ishida, H. Vibrational assignments of N,N-bis(3,5-dimethyl-2-hydroxybenzyl)methylamine in the fingerprint region. *Spectrochim. Acta Part A Mol. Biomol. Spectrosc.* **1995**, *51*, 855–867. [CrossRef]
45. Dogan, Y.E.; Satilmis, B.; Uyar, T. Synthesis and characterization of bio-based benzoxazines derived from thymol. *J. Appl. Polym. Sci.* **2019**, *136*, 47371. [CrossRef]
46. Kudoh, R.; Sudo, A.; Endo, T. A Highly Reactive Benzoxazine Monomer, 1-(2-Hydroxyethyl)-1,3-Benzoxazine: Activation of Benzoxazine by Neighboring Group Participation of Hydroxyl Group. *Macromolecules* **2010**, *43*, 1185–1187. [CrossRef]
47. Zhang, L.; Rowan, S.J. Effect of Sterics and Degree of Cross-Linking on the Mechanical Properties of Dynamic Poly(alkylurea–urethane) Networks. *Macromolecules* **2017**, *50*, 5051–5060. [CrossRef]
48. Li, W.; Xiao, L.; Huang, J.; Wang, Y.; Nie, X.; Chen, J. Bio-based epoxy vitrimer for recyclable and carbon fiber reinforced materials: Synthesis and structure-property relationship. *Compos. Sci. Technol.* **2022**, *227*, 109575. [CrossRef]
49. Adjaoud, A.; Trejo-Machin, A.; Puchot, L.; Verge, P. Polybenzoxazines: A sustainable platform for the design of fast responsive and catalyst-free vitrimers based on trans-esterification exchanges. *Polym. Chem.* **2021**, *12*, 3276–3289. [CrossRef]
50. Su, C.; Wu, W.; Li, Z.; Guo, Y. Prediction of film performance by electrochemical impedance spectroscopy. *Corros. Sci.* **2015**, *99*, 42–52. [CrossRef]
51. Mohamad, A.B.; Kadhum, A.A.H.; Al-Amiery, A.A.; Ying, L.C.; Musa, A.Y. Synergistic of a coumarin derivative with potassium iodide on the corrosion inhibition of aluminum alloy in 1.0 M H_2SO_4. *Met. Mater. Int.* **2014**, *20*, 459–467. [CrossRef]
52. Møller, V.B.; Dam-Johansen, K.; Frankær, S.M.; Kiil, S. Acid-resistant organic coatings for the chemical industry: A review. *J. Coat. Technol. Res.* **2017**, *14*, 279–306. [CrossRef]
53. Miszczyk, A.; Darowicki, K. Water uptake in protective organic coatings and its reflection in measured coating impedance. *Prog. Org. Coat.* **2018**, *124*, 296–302. [CrossRef]
54. Wang, L.; Snihirova, D.; Deng, M.; Wang, C.; Vaghefinazari, B.; Wiese, G.; Langridge, M.; Höche, D.; Lamaka, S.V.; Zheludkevich, M.L. Insight into physical interpretation of high frequency time constant in electrochemical impedance spectra of Mg. *Corros. Sci.* **2021**, *187*, 109501. [CrossRef]